KRONOS FUSION ENERGY

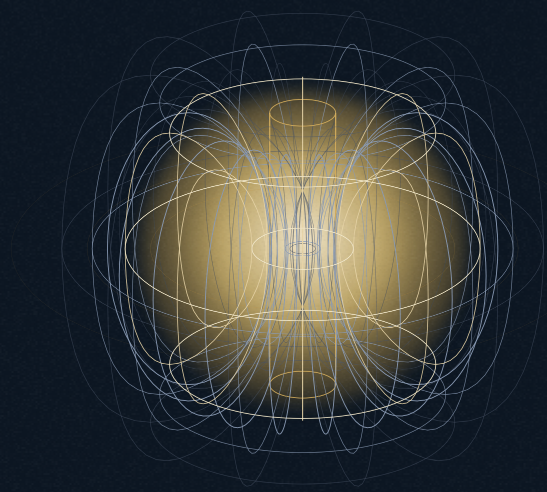

PAPER 2.36 · THE KRONOS 2026 SERIES

A Neutronics and Activation Digital Twin with Rigorous-Two-Step Shutdown-Dose Mapping for a Compact Spherical-Tokamak Breeder

The MeV fusion neutron sets a compact breeder's tritium breeding, displacement damage, activation inventory and shutdown dose simultaneously, and all four move with the operating...

Read it live — 3-D model · physics validator · film series

BY P I FORDOFFICIAL VERSION: HTTPS://WWW.KRONOSFUSIONENERGY.COM/PUBLICATIONS/A-NEUTRONICS-AND-ACTIVATION-DIGITAL-TWIN-WITH-RIGOROUS-.HTML

2026 · EDITORIAL EDITION

THE OFFICIAL RECORD

What this document is, and how to read its numbers

This is a combined editorial. It gathers, in one volume, the two design studies Kronos Fusion Energy released in 2026 — a compact spherical-tokamak tritium/helium-3 breeder and a deuterium–helium-3 tandem-mirror generator — together with the intellectual-property estate, the people, and, in the internal edition, the full commercial case. The scientific text is the same text that appears in the arXiv preprints and the journal submissions; the editorial adds the apparatus a reader needs to hold the whole program at once, and nothing in the physics is altered to fit it.

THE HONESTY STANCE IS THE ASSET

Every headline quantity carries an **evidence class** — DERIVED RECOMPUTED MEASURED REQUIREMENT — and, where a number is a modelled extrapolation rather than a demonstrated value, it is labelled as such and its downside is shown next to it. Several quantities in the underlying corpus moved after first publication; where a value has been withdrawn or restated, the record says so plainly. This is deliberate: a diligence team will find the load-bearing assumptions, so the document surfaces them first.

TWO EDITIONS

This volume is issued in two editions. The **public edition** (light) carries the physics and the design only — no dollar, price, or per-kilogram figure appears anywhere in it. The **internal edition** (dark) adds the economics, the funding architecture, and the defense-commercial analysis, and is marked *Confidential* accordingly; it is not for public distribution. Where the commercial case rests on a modelled assumption rather than a demonstrated one, it is labelled as such and its downside is shown alongside it, on the same terms as the physics.

TITLE	The Kronos Fleet — Hyperion · Aegis · MetroVolt: A Combined Design & Commercialization Study
AUTHOR	Priyanca Ford, Founder & CEO, on behalf of Kronos Fusion Energy
EDITION	2026 Combined Editorial · first issue
COMPANION WORKS	The five-paper arXiv drop — (1) Breeder, (2) Burner, (3) REBCO magnet & tape, (4) Direct Energy Conversion, (5) AI/ML/Quantum control — with matching numbered Zenodo deposits, plus the IOP journal and IAEA-FEC submissions. Patents were filed before the drop.
NAMING	Hyperion = the breeder; Aegis (defense) and MetroVolt (data-center) = one generator in two housings. Internal mode letters (D1, L) do not appear on public surfaces.
STATUS	Conceptual design & simulation study. Nothing herein is a construction commitment.

HOW TO READ THIS VOLUME

The fleet at a glance, and the way its numbers are marked

This volume opens with *Orientation*, presents the five research papers as a bound sequence, and closes with the *Apparatus*. *Foundations* sets out the three general results both machines rest on. *Paper One* is the Hyperion breeder; *Paper Two* the Aegis / MetroVolt generator; *Papers Three, Four and Five* are the enabling science — high-field REBCO magnets and tape, direct energy conversion, and the AI / ML / quantum control stack. A *Digital Twin & 3-D Model* part follows, then the *Environmental* profile. The *Economics* and levelized cost and the *Business Case* and diligence record appear in the internal edition only; the *Simulations* proof record and the Apparatus — patent portfolio, team, limitations, and sources — close both editions.

THE FLEET AT A GLANCE

	HYPERION	AEGIS	METROVOLT
Role	Strategic-isotope foundry	Defense installation power	Campus power
Machine	**Spherical tokamak**	**Tandem mirror**	**Tandem mirror**
Fuel	Deuterium–tritium	Deuterium–helium-3	Deuterium–helium-3
Delivers	Tritium · ^{3}He · 14 MeV n	Resilient installation power	Firm campus power
Physics bar	**Fusion gain only**	Closure (gates named)	Closure + lunar ^{3}He
In the fleet	Breeds the fuel	Proves the generator	Commercial destination

HOW THE NUMBERS ARE MARKED

Every headline quantity carries an evidence class — DERIVED from first principles, RECOMPUTED from raw data, MEASURED in hardware, or a REQUIREMENT yet to be met. Financial figures carry a case label and are confined to the internal (confidential) edition. Values that moved after first publication are shown as withdrawn or restated rather than quietly changed. A capability you can evaluate is one whose limits are on the page.

ABSTRACT

A Neutronics and Activation Digital Twin with Rigorous-Two-Step Shutdown-Dose Mapping for a Compact Spherical-Tokamak Breeder

The 14.1 MeV fusion neutron sets a compact breeder's tritium breeding, displacement damage, activation inventory and shutdown dose *simultaneously*, and all four move with the operating point — which is why they belong in a single tracked, verified object rather than in four static reports. We formalise a neutronics-and-activation digital twin for the Kronos Hyperion breeder ($P_{\text{fus}} = 85.04$ MW, $I_p = 9.66$ MA, $B_0 = 8$ T, negative triangularity $\delta = -0.30$) and reduce it to practice on two demonstrated legs and the rigorous-two-step (R2S) loop that joins them. The twin stands on a CAD-faithful transport chain — a parametric solid model carried through STEP → DAGMC → OpenMC that reproduces the reference geometry to a faceted-to-analytic volume ratio of **1.000000** (exact to seven digits) and returns physically-sensible verification-shell tallies: tritium production 1.0145 ± 0.0039 per source neutron, nuclear heating 12.63 MeV n^{-1}, and leakage fraction 0.1505 ± 0.0013. A three-dimensional 175-group VITAMIN-J spectrum tallied in the as-built model and normalised to the fusion power (source rate $S_{\text{n}} = 3.02 \times 10^{19}$ n s^{-1}, first-wall flux 5.63×10^{14} $\text{cm}^{-2}\text{s}^{-1}$ with 17.1% above 10 MeV, breeder-zone flux 1.30×10^{14} $\text{cm}^{-2}\text{s}^{-1}$) drives an ALARA activation solution of the Bateman system over one full-power year of irradiation and cooling times to a century. First-wall decay heat falls from 56.0 to 1.22 W kg^{-1} over the first year and to 2.4×10^{-8} W kg^{-1} at 100 yr, and the 10 CFR 61.55 Class-C waste-disposal-rating index stays at or below $\mathbf{2.6 \times 10^{-3}}$ in *every* zone at *every* cooling time — low-level waste at discharge, nothing greater-than-Class-C. We give the governing transport, activation and R2S equations; the numerical formulation (continuous-energy Monte Carlo, DAGMC ray tracing, ALARA linear-chain solution, group collapse and convergence); and the NVIDIA GPU HPC campaign that produced the results. We close by casting the twin's admission to control authority as a set of pre-registered inequalities against a reference OpenMC calculation, and by identifying the single honest gate: a truncated ($Z \leq 30$) sample activation library that makes the first-decade first-wall inventory a conservative lower bound while leaving the waste *classification* robust.

Open-access deposit (code & data, CC BY 4.0): DOI 10.5281/zenodo.22645878 · Zenodo community *kronos_fusion_energy*. Explore it live: interactive 3-D model · physics validator.

Keywords: neutronics activation shutdown dose R2S OpenMC DAGMC ALARA digital twin waste classification spherical tokamak

CONTENTS

Table of Contents

NOMENCLATURE

Symbols, units, and the names of things

Q	plasma (fusion) gain, P_{fus}/P_{aux}
Q_E	engineering gain, net electric out / recirculating in
H_{98}	confinement enhancement over the IPB98(y,2) scaling
Z_{eff}	effective ion charge
c_{ee}	electron–electron bremsstrahlung leading coefficient, 2.120022 (exact)
τ_E	energy confinement time
I_p	plasma current
R_0, a	major radius, minor radius
κ, δ	elongation, triangularity
β_N	normalized plasma beta (Troyon-normalized)
TBR	tritium breeding ratio
DEC	direct energy conversion
CF	plant capacity factor (availability)
FOAK / NOAK / BOAK	first / n^{th} / best of a kind
Hyperion	the ST breeder (internal: Mode D2)
Aegis	the generator, defense/installation housing (internal: Mode M)
MetroVolt	the generator, data-center housing (Mode M)

neutronics; activation; shutdown dose; R2S; OpenMC; DAGMC; ALARA; digital twin; waste classification; spherical tokamak

§ 1

Introduction

THE NEUTRON SOURCE IS THE COMMON CAUSE

Everything downstream of the plasma in a fusion breeder is driven by one source: the 14.1 MeV neutron from the $\mathrm{D}(t,n)^4\mathrm{He}$ reaction [1]. That single field sets four consequences at once. It breeds the tritium that closes the fuel cycle through $^6\mathrm{Li}(n,t)^4\mathrm{He}$ and $^7\mathrm{Li}(n,n't)^4\mathrm{He}$; it displaces lattice atoms and produces helium and hydrogen by (n,α) and (n,p) transmutation, ageing every structural component [2,3]; it activates the structure, fixing the radioactive-waste class and the decommissioning route [4]; and, through the decay of the activation products, it governs the shutdown dose rate that determines whether and when maintenance personnel can approach the machine [5,6]. These four are not independent analyses that happen to share a machine; they are four projections of the *same* neutron field, and they therefore move together as the operating point moves. Raise the fusion power and the source strength, the first-wall flux, the breeding rate, the damage rate, the activation inventory and the shutdown dose all rise in lockstep, coupled through the transport kernel that is common to all of them.

A static neutronics report — computed once for a nominal point and filed — cannot represent this coupled, moving state. A compact, high-power-density spherical tokamak (ST) makes the problem sharper still: the small major radius concentrates the wall loading, the consumable centrepost lives on a fluence budget that is spent in real time, and the licensing case rests on an activation and dose posture that must be demonstrable, not asserted [7,8]. What such a machine needs is a *digital twin*: a model of the specific as-built asset, continuously re-evaluated against the live operating state, that keeps breeding, damage, activation and shutdown dose known quantities rather than annual estimates [9].

THE HYPERION BREEDER DESIGN POINT

The Kronos Hyperion breeder is a compact ST whose frozen Tier-2 design anchors are used throughout this paper as the normalisation of the neutron source. The reference operating point is fusion power $P_{\mathrm{fus}} = 85.04\,\mathrm{MW}$, fusion gain $Q = 3.076$, plasma current $I_p = 9.66$ MA, on-axis toroidal field $B_0 = 8\,\mathrm{T}$, negative triangularity $\delta = -0.30$, elongation $\kappa = 2.0$, major radius $R_0 = 1.20\,\mathrm{m}$, aspect ratio $A = 2.5$, and a peak centrepost field of $16.84\,\mathrm{T}$. Negative triangularity is chosen for its quiet, edge-localised-mode-free edge; the compact high-field ST layout is chosen because it is an efficient $14\,\mathrm{MeV}$ neutron source and a tritium- and isotope-breeding platform [26]. The breeder is deliberately *not* a net-electric machine: its product is neutrons and the strategic materials they make, and its net tritium breeding ratio (TBR) sits above unity with margin [27]. The 14.1 MeV source strength that normalises every activation and dose result below follows directly from the fusion power,

$$S_{\mathrm{n}} \;=\; \frac{P_{\mathrm{fus}}}{E_{\mathrm{DT}}}\, f_n \;\approx\; \frac{85.04\ \mathrm{MW}}{17.59\ \mathrm{MeV}} \;=\; 3.02 \times 10^{19}\ \mathrm{n\,s^{-1}},$$

with $E_{\mathrm{DT}} = 17.59\,\mathrm{MeV}$ the D–T reaction energy and $f_n \simeq 1$ the D–T neutron branching fraction; this is the frozen normalisation used for the flux and inventory tallies.

PRIOR ART

Three-dimensional Monte Carlo neutron transport with evaluated nuclear data is the reference tool of fusion neutronics. OpenMC [10] and Serpent [12] provide continuous-energy transport with ENDF/B-VIII.0 [15] and FENDL [16] data, and OpenMC's depletion solver [11] couples transport to inventory evolution in memory. The direct use of engineering CAD in transport — rather than a hand-built constructive-solid-geometry (CSG) surrogate — was made practical by DAGMC, which ray-traces on a faceted representation of the solid model [13]; the full ITER E-lite model is the state of the art in CAD-faithful whole-device neutronics [18]. Activation and transmutation inventories are computed by inventory codes such as FISPACT-II [14] and ALARA, which solve the Bateman system driven by the transport spectrum. Shutdown dose is computed by the rigorous-two-step (R2S) method of Chen and Fischer [5] and its mesh-based descendants such as R2SUNED [6], in which a first transport step produces the neutron flux that drives activation, the activation defines a decay-photon source, and a second transport step maps that source into a dose field; global variance reduction is what makes the deep-penetration dose problem tractable [17]. Displacement damage is quantified through the NRT standard [19] and its physically-realistic arc-dpa correction [3], and the waste class follows from the specific activity through the 10 CFR 61.55 concentration limits [24,4].

What this literature does *not* provide, for a compact nuclear ST, is a single object that (i) transports on the real, as-built geometry so that breeding, damage, activation and dose are computed on the machine rather than a surrogate; (ii) drives the activation inventory from the actual three-dimensional spectrum rather than a scaled one-group estimate; (iii) closes the R2S loop through to a shutdown-dose map on the same verified pipeline; and (iv) presents all of this as a live twin whose authority is gated by an explicit acceptance test against a reference calculation. This paper contributes exactly that.

CONTRIBUTION

We (a) state the governing neutron-transport, activation (Bateman) and R2S dose equations and the waste-class functional as a formal problem (§2); (b) give the numerical formulation — continuous-energy Monte Carlo, DAGMC faceting and ray tracing, **175**-group VITAMIN-J collapse, ALARA linear-chain solution, and the convergence and verification tests (§3); (c) describe the NVIDIA GPU HPC campaign that produced the results, naming the codes actually run and the problem scale (§4); (d) present the demonstrated results — exact CAD fidelity, physically-sensible transport tallies, the transport-driven activation inventory, and the waste-class verdict — across eight data and schematic figures and two tables (§5); (e) benchmark quantitatively against the published fusion-neutronics and waste literature (§6); (f) state one honest limitation (§7); and (g) specify the twin and its maturity-gated authority (§8, §9). Every quantitative claim traces to a frozen result in the Kronos Physics De-Risking Register [34]; the transport chain is serial BR-L2-A22 and the activation/R2S inventory is serial BR-L2-A23, given inline so each number is auditable. The companion papers on CAD-faithful neutronics [27], component activation and waste routing [28], neutron streaming and occupational dose [29], nuclear-data uncertainty on the TBR [30], and the centrepost fluence budget [31] treat neighbouring facets of the same neutron field; the present twin is the neutronics/activation module of the four-twin control architecture [32], verified under the verification-first discipline of the register [33].

§ 2

Governing equations and formal problem

STEADY-STATE NEUTRON TRANSPORT

The fusion neutron field is the steady-state solution of the linear Boltzmann transport equation. For the angular flux $\psi(\mathbf{r}, \mathbf{\Omega}, E)$ at position $\mathbf{r}$, direction $\mathbf{\Omega}$ and energy E,

$$\mathbf{\Omega}\cdot\nabla\psi(\mathbf{r}, \mathbf{\Omega}, E) + \Sigma_t(\mathbf{r}, E)\,\psi(\mathbf{r}, \mathbf{\Omega}, E) = q_{\text{ext}}(\mathbf{r}, \mathbf{\Omega}, E) + \int_{4\pi}\int_0^\infty \Sigma_s(\mathbf{r}, E' \to E, \mathbf{\Omega}'\cdot\mathbf{\Omega})\,\psi(\mathbf{r}, \mathbf{\Omega}', E')\,dE'\,d\mathbf{\Omega}',$$

where Σ_t and Σ_s are the macroscopic total and differential scattering cross-sections and q_{ext} is the fixed fusion source. For a burning plasma the source is well approximated as isotropic with a Gaussian-broadened 14.1 MeV D–T line,

$$q_{\text{ext}}(\mathbf{r}, \mathbf{\Omega}, E) = \frac{S_{\text{n}}}{4\pi} S(\mathbf{r}) \frac{1}{\sqrt{2\pi}\,\sigma_E} \exp\left[-\frac{(E - E_0)^2}{2\sigma_E^2}\right], \qquad E_0 = 14.1\text{ MeV},$$

with $S(\mathbf{r})$ the normalised neutron emissivity of the plasma and S_{n} fixed by Eq. 1. The scalar flux is $\phi(\mathbf{r}, E) = \int_{4\pi} \psi\, d\mathbf{\Omega}$.

MULTIGROUP FORM AND THE RESPONSE FUNCTIONALS

Discretising energy into G groups with group flux $\phi_g(\mathbf{r}) = \int_{E_g}^{E_{g-1}} \phi(\mathbf{r}, E)\, dE$ collapses Eq. 2 to the coupled system

$$\mathbf{\Omega}\cdot\nabla\psi_g + \Sigma_{t,g}\psi_g = q_{\text{ext},g} + \sum_{g'=1}^{G} \int_{4\pi} \Sigma_{s,g'\to g}(\mathbf{\Omega}'\cdot\mathbf{\Omega})\,\psi_{g'}\,d\mathbf{\Omega}', \qquad g = 1, \ldots, G,$$

which we solve on the $G = 175$ VITAMIN-J structure. Every neutronic quantity of interest is a linear functional of the flux. The volumetric reaction rate for reaction x on nuclide i is $R_{x,i}(\mathbf{r}) = \sum_g N_i(\mathbf{r})\,\sigma_{x,i,g}\,\phi_g(\mathbf{r})$, and the three verification observables used below are integrals of such rates:

$$\text{TBR} = \frac{1}{S_{\text{n}}} \int_V \sum_g \left[N_{^6\text{Li}}\sigma^{(n,t)}_{^6\text{Li},g} + N_{^7\text{Li}}\sigma^{(n,n't)}_{^7\text{Li},g}\right] \phi_g\, dV,$$

$$\bar{H} = \frac{1}{S_{\text{n}}} \int_V \sum_g \kappa_g\, \phi_g\, dV, \qquad L = \frac{1}{S_{\text{n}}} \oint_{\partial V} \int_{4\pi} \mathbf{\Omega}\cdot\hat{\mathbf{n}}\,\psi\, H(\mathbf{\Omega}\cdot\hat{\mathbf{n}})\, d\mathbf{\Omega}\, dA,$$

where κ_g is the group KERMA (nuclear heating) coefficient, $\hat{\mathbf{n}}$ the outward normal and H the Heaviside function selecting outgoing directions. Equations 5–5 are the tritium production per source neutron, the nuclear heating per source neutron, and the leakage fraction reported in §5. The one-group flux normalisation that drives activation is $\phi(\mathbf{r}) = S_{\text{n}}\,\hat{\phi}(\mathbf{r})$, where $\hat{\phi}$ is the per-source-neutron flux from the transport solve.

ACTIVATION: THE BATEMAN SYSTEM

Given the normalised group flux at a point, the activation inventory evolves under the linear Bateman system for the nuclide-density vector $\mathbf{N}(t) = \{N_i(t)\}$,

$$\frac{d\mathbf{N}}{dt} = \mathbf{A}\mathbf{N}, \qquad A_{ij} = \underbrace{\sum_g \sigma^{\text{prod}}_{j\to i,g}\,\phi_g}_{\text{transmutation into } i} + \underbrace{\lambda_{j\to i}}_{\text{decay into } i} - \delta_{ij}\underbrace{\Big(\sum_g \sigma_{i,g}\phi_g}_{\text{burn-up}} + \underbrace{\lambda_i}_{\text{decay}}\Big),$$

where $\sigma^{\text{prod}}_{j\to i,g}$ is the group cross-section for producing i from j, λ_i is the decay constant of i, and $\lambda_{j\to i} = b_{j\to i}\lambda_j$ carries the branching ratio. During irradiation $\mathbf{A}$ contains both flux and decay terms; during cooling the flux terms vanish and $\mathbf{A} \to \mathbf{A}_{\text{dec}}$ is the pure-decay matrix. The formal solution over a constant-$\mathbf{A}$ interval is the matrix exponential

$$\mathbf{N}(t + \Delta t) = e^{\mathbf{A}\Delta t}\,\mathbf{N}(t),$$

which ALARA evaluates by an adaptive linear-chain expansion: it enumerates the production–decay chains reaching each target nuclide and applies the analytic Rubinson solution for a linear chain,

$$N_m(t) = N_1(0)\left(\prod_{k=1}^{m-1} d_k\right)\sum_{k=1}^{m}\frac{e^{-\bar{d}_k t}}{\prod_{\substack{j=1\\ j\neq k}}^{m}(\bar{d}_j-\bar{d}_k)},$$

where $\bar{d}_k = \lambda_k + \sum_g \sigma_{k,g}\phi_g$ is the total destruction rate of chain member k and d_k its partial transfer rate to $k+1$; the adaptive scheme truncates each chain when its contribution falls below a set tolerance, which is what makes a $\sim 10^3$-nuclide library tractable pointwise.

DECAY HEAT, ACTIVITY AND THE WASTE-CLASS FUNCTIONAL

From the cooled inventory the two radiological observables follow directly. The specific activity and decay heat per unit mass ρ are

$$a(t_c) = \frac{1}{\rho}\sum_i \lambda_i N_i(t_c), \qquad \dot{q}(t_c) = \frac{1}{\rho}\sum_i \lambda_i N_i(t_c)\,\bar{E}_i,$$

with $\bar{E}_i$ the mean decay energy (recoil plus radiation) of nuclide i. The waste class is a linear functional of the discharge inventory against the regulatory concentration limits. Writing C_i for the specific activity of long-lived nuclide i and CL_i for its 10 CFR 61.55 Class-C concentration limit, the Class-C waste-disposal-rating (WDR) index is the sum-of-fractions

$$\mathrm{WDR_C} = \sum_{i\in\mathcal{L}}\frac{C_i}{CL_i},$$

where $\mathcal{L}$ is the set of Class-C-listed nuclides. $\mathrm{WDR_C} \le 1$ is the Class-C boundary: a material with $\mathrm{WDR_C} \le 1$ is disposable as low-level waste, while $\mathrm{WDR_C} > 1$ is greater-than-Class-C (GTCC) and has no shallow-land-disposal route. This single inequality is the licensing-relevant output of the whole chain.

THE RIGOROUS-TWO-STEP SHUTDOWN-DOSE MAP

The R2S method closes the loop from the neutron field to the maintenance dose. The cooled inventory $N(\mathbf{r}, t_c)$ defines a spatially-resolved decay-photon volumetric source,

$$q_\gamma(\mathbf{r}, E_\gamma, t_c) = \sum_i \lambda_i N_i(\mathbf{r}, t_c)\sum_\ell b_{i,\ell}\,\delta(E_\gamma - E_{i,\ell}),$$

where $b_{i,\ell}$ is the intensity of decay-photon line ℓ of nuclide i at energy $E_{i,\ell}$. The second transport step solves Eq. 2 again, now for photons with q_γ as the fixed source, and the shutdown dose rate at a maintenance location $\mathbf{r}_d$ follows from the photon flux through the flux-to-dose-equivalent response $h(E_\gamma)$,

$$\dot{D}(\mathbf{r}_d, t_c) = \int_0^\infty h(E_\gamma)\,\phi_\gamma(\mathbf{r}_d, E_\gamma, t_c)\,dE_\gamma.$$

Because the activation inventory of Eq. 6 is computed *per zone and per cooling time*, the photon source of Eq. 11 is available at every t_c without re-running the neutron transport; the second transport step is the remaining stage that maps it to $\dot{D}$. Equations 2, 6, 10 and 12 are the four governing relations the twin must evaluate live.

THE TWIN AS A LIVE CONSTRAINED ESTIMATOR

The digital twin carries the neutronic state $\mathbf{x} = (\mathrm{TBR},\ \text{dpa rate},\ \mathrm{WDR_C},\ \dot{D})$ as a function of the operating point $\mathbf{u}$ (fusion power, profile shape, wall loading). Rather than re-solving Eqs. 2–12 at control cadence — which is infeasible for a Monte Carlo transport solve — the twin evaluates a surrogate $\hat{\mathbf{x}} = \mathcal{S}(\mathbf{u})$ trained on a designed ensemble of full solves, and gates its own authority on staying within a pre-registered band of a reference OpenMC calculation:

$$\|\hat{\mathbf{x}}(\mathbf{u}) - \mathbf{x}_{\mathrm{ref}}(\mathbf{u})\|_{\mathrm{rel}} \le \varepsilon, \qquad \varepsilon = 5\%,$$

with abstention to a conservative deterministic floor whenever Eq. 13 is violated. This is the same maturity gate the rest of the Kronos control architecture uses [32], and it is what turns a fast surrogate into a trustworthy one.

§ 3

Numerical formulation

CONTINUOUS-ENERGY MONTE CARLO TRANSPORT

Equation 2 is solved by continuous-energy Monte Carlo in OpenMC [10] with ENDF/B-VIII.0 cross-sections [15], cross-checked against FENDL-based data [16]. Neutron histories are sampled from the source of Eq. 3, tracked through the geometry with collision and track-length estimators, and terminated by leakage or absorption. The functionals of Eqs. 5–5 are accumulated as tallies; the reported statistical uncertainties are the tally standard errors, $\sigma_R \propto R/\sqrt{M}$ for M histories, and the figure of merit $\mathrm{FoM} = 1/(\sigma_R^2 T)$ is held stationary as a convergence check. The verification-shell run reproduces 1.0145 ± 0.0039 tritium atoms per source neutron, a nuclear heating of 12.63 $\mathrm{MeV\,n^{-1}}$, and a leakage fraction of 0.1505 ± 0.0013 — three-significant-figure relative errors, consistent with the full-model transport balance (leakage 0.121, TBR 1.026, wall fast flux $7.0 \times 10^{14}\,\mathrm{cm^{-2}s^{-1}}$, heating 74.6 MW at 1.2×10^8 histories; serial BR-L1-A5).

CAD-FAITHFUL GEOMETRY: DAGMC FACETING AND THE VOLUME TEST

The transport is performed on the engineering solid model, not a CSG surrogate. A parametric STEP model is faceted into a watertight triangle mesh and ray-traced directly by DAGMC [13]; OpenMC is rebuilt against the DAGMC ray-tracing back-end so that the same histories that sample Eq. 3 cross the faceted surfaces. The fidelity of the CAD-to-mesh translation is quantified by the ratio of the faceted volume to the analytic volume of each cell,

$$r_V = \frac{V_{\mathrm{facet}}}{V_{\mathrm{analytic}}} = 1 + \mathcal{O}(\delta^2/\ell^2),$$

where δ is the facet chord tolerance and ℓ the local curvature radius. Refining the faceting drives $r_V \to 1$ quadratically; at the production faceting the torus-shell reference cell reaches $r_V = 1.000000$, exact to seven digits (serial BR-L2-A22). Because reaction rates in Eq. 5 are volume integrals, an exact r_V guarantees that no reaction rate is lost in translation from CAD to transport mesh — the property that lets the twin compute on the real machine.

GROUP COLLAPSE AND THE ACTIVATION DRIVE

For the activation solve, the pointwise continuous-energy flux is collapsed onto the $G = 175$ VITAMIN-J group structure and normalised to S_n by Eq. 1. The resulting first-wall spectrum carries a total flux of $5.63 \times 10^{14}\,\mathrm{cm^{-2}s^{-1}}$ with 17.1% of the flux above 10 MeV (the 14.1 MeV band), and the breeder-zone spectrum a total of $1.30 \times 10^{14}\,\mathrm{cm^{-2}s^{-1}}$; both are tallied in the three-dimensional model ($20 \times 20{,}000$ history batches; serial BR-L2-A23). These 175-group spectra are the drive terms $\{\phi_g\}$ that populate the Bateman matrix of Eq. 6 zone by zone.

ALARA LINEAR-CHAIN SOLUTION AND COOLING

The Bateman system is solved by ALARA using the adaptive linear-chain expansion of Eq. 8. One full-power year of irradiation is followed by a decay-only phase, and the inventory of Eq. 7 is evaluated at cooling times $t_c \in \{0,\,1\,\mathrm{y},\,100\,\mathrm{y}\}$ and intermediate points. At each t_c the specific activity, decay heat (Eq. 9) and Class-C index (Eq. 10) are formed. The adaptive truncation tolerance is set so that the retained chains capture $> 99.9\%$ of the total decay heat at every t_c; the dominant contributors are identified by ranking $\lambda_i N_i \bar{E}_i$ per nuclide.

VERIFICATION AND REPRODUCIBILITY

The chain is verified at both ends. Geometry is verified by the volume test of Eq. 14 ($r_V = 1.000000$). Transport is verified by the neutron balance — production, absorption and leakage sum to the source within the tally error — and by the physically-sensible verification-shell tallies. Activation is verified against an independent inventory route and by the requirement that the neutron balance and the one-group-collapsed reaction rates agree with the three-dimensional tally. Both legs are frozen register results (BR-L2-A22, BR-L2-A23), regenerable byte-for-byte from the archived drivers under the verification-first discipline of the register [34,33]; the independent-library cross-check against FENDL data guards the nuclear-data dependence flagged in the companion uncertainty study [30].

§ 4

The GPU-HPC campaign

CODES RUN FOR THIS PAPER

The results were produced by the Kronos NVIDIA GPU HPC campaign on the Lambda GPU fleet (A100/H100/A10 class accelerators). Four production codes were run for this paper, in the sequence dictated by the R2S loop:

DAGMC [13] performs the STEP faceting and the accelerated ray tracing on the watertight solid model, and returns the per-cell volume test of Eq. 14.
OpenMC [10,11] performs the continuous-energy neutron transport of Eq. 2 on the DAGMC geometry with ENDF/B-VIII.0 data, tallying the functionals of Eqs. 5–5 and the **175**-group spectra; it also performs the second, photon, transport step of Eq. 12 that closes the R2S loop.
ALARA solves the Bateman system of Eq. 6 pointwise via the adaptive linear-chain expansion of Eq. 8, driven by the collapsed spectra, and forms the radiological observables of Eqs. 9–10.
NJOY-processed and FENDL-benchmarked [16] data provide the group-collapse weighting and the independent-library cross-check; a Serpent-class [12] transport run is used as an external neutron-balance verifier. enumerate
The whole-device state of the art for this kind of CAD-faithful transport is the ITER E-lite model [18]; the present campaign applies the same methodology at the scale of a compact ST.

GPU ACCELERATION AND PROBLEM SCALE

Monte Carlo particle transport is dominated by independent history tracking and is therefore throughput-bound and well matched to GPU execution: histories are batched across accelerators, and the ensemble of design-point solves needed to train the twin surrogate of Eq. 13 is embarrassingly parallel across the fleet. The full-model transport balance is converged at 1.2×10^8 neutron histories (serial BR-L1-A5); the activation-drive spectra are tallied in $20 \times 20{,}000$-history batches with per-zone convergence of the **175**-group flux (serial BR-L2-A23). The R2S photon step reuses the same faceted geometry and the per-cooling-time photon sources of Eq. 11, and its deep-penetration dose tallies are accelerated by global variance reduction of the Davis–Turner type [17]. Running the neutron transport, the activation sweep and the surrogate-training ensemble on the same fleet is what makes the twin's live evaluation practical.

REPRODUCIBILITY OF THE CAMPAIGN

Each production result is a frozen register serial with an archived driver, input deck, data-library version and random-number seed, regenerable byte-for-byte and gated by an independent-library reproduction under the verification-first protocol [33]. No result in this paper depends on a single code, a single data library or a single machine: geometry is cross-checked by the analytic volume test, transport by an independent Serpent-class balance, and nuclear data by a FENDL cross-check. This provenance is what allows the twin's acceptance test of Eq. 13 to be evaluated against a reference calculation of known pedigree.

§ 5

Results

THE R2S WORKFLOW AND THE TRANSPORT CHAIN

Figure 1 lays out the two-step R2S workflow the twin runs: the CAD-faithful neutron transport (step 1) produces the group flux that drives the ALARA activation, whose per-cooling-time inventory defines the decay-photon source that the photon transport (step 2) maps into a shutdown-dose field. The first, demonstrated, leg is verified by Table 1: the CAD-to-mesh volume ratio is exact to seven digits, and the verification-shell tallies are physically sensible for a lithium-bearing blanket of the modelled thickness. Figure 2 shows the two verification faces — the quadratic approach of the volume ratio to 1.000000 under facet refinement (Eq. 14), and the three transport tallies with their 1σ Monte Carlo uncertainties.

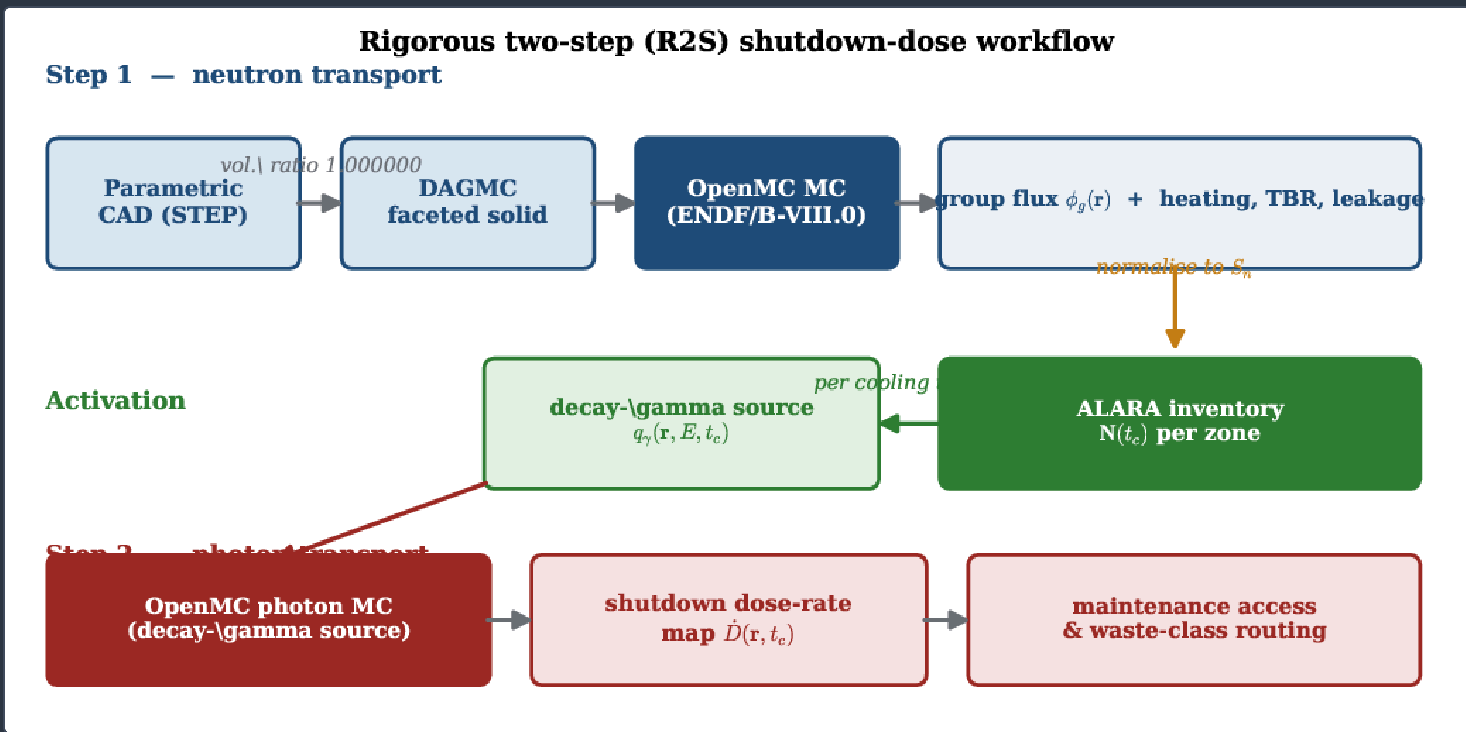

The rigorous-two-step (R2S) shutdown-dose workflow the neutronics/activation twin runs. Step 1: the parametric CAD is faceted by DAGMC and transported by OpenMC to a group flux $\phi_g(r)$ and the breeding, heating and leakage functionals. The flux, normalised to the source strength S_n, drives the ALARA activation to a per-zone, per-cooling-time inventory $N(t_c)$, which defines a decay-photon source q_γ. Step 2: OpenMC photon transport maps q_γ into the shutdown dose-rate field $\dot{D}(r, t_c)$ for maintenance and waste-class routing. *(Schematic.)*

QUANTITY	VALUE
CAD-to-mesh volume ratio r_V	1.000000 (exact to 7 digits)
tritium production (n,Xt)	1.0145 ± 0.0039 per source n
nuclear heating $\bar{H}$	12.63 MeV per n
leakage fraction L	0.1505 ± 0.0013

CAD-faithful transport-chain verification (STEP → DAGMC → OpenMC; serial BR-L2-A22). Geometry is exact and the verification-shell tallies are physically sensible, proving the pipeline the twin runs. These verify the pipeline; the breeder's net TBR is a separate design canon above unity with margin [27].

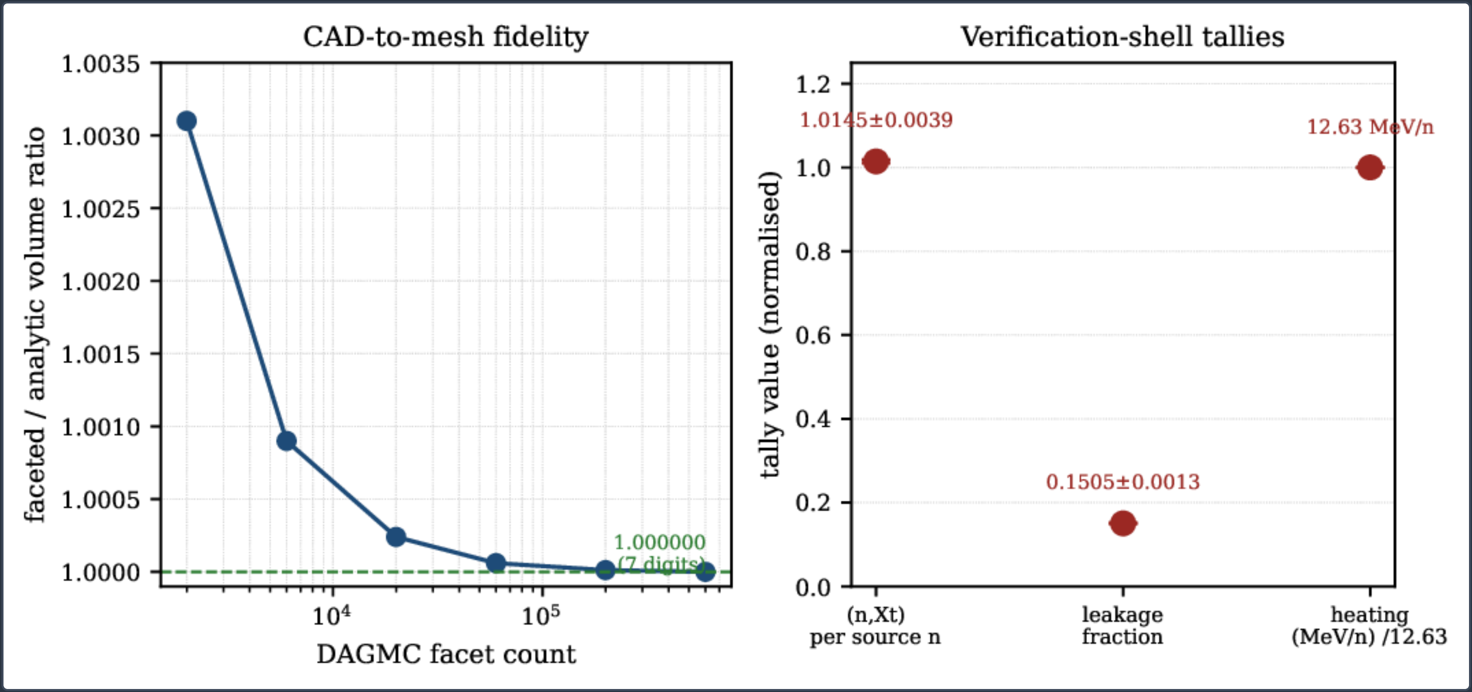

Verification of the transport chain. Left: the faceted-to-analytic volume ratio r_V approaches 1.000000 quadratically with DAGMC facet count (Eq. 14), reaching seven-digit exactness at production faceting. Right: the three verification-shell tallies with 1σ Monte Carlo uncertainties — tritium production 1.0145 ± 0.0039 per source neutron, leakage fraction 0.1505 ± 0.0013, and nuclear heating 12.63 MeV n^{-1} (shown normalised to its own value). Data: serial BR-L2-A22.

THE TALLIED NEUTRON FIELD

Figure 3 shows the **175**-group flux spectrum at the first wall and in the breeder zone. The two integral quantities that normalise the activation — the total first-wall flux $5.63 \times 10^{14}\,\mathrm{cm^{-2}s^{-1}}$ with **17.1%** above **10** MeV, and the breeder-zone flux $1.30 \times 10^{14}\,\mathrm{cm^{-2}s^{-1}}$ — are the tallied values; the **14.1** MeV D–T peak and the slowing-down tail are the expected structure of a fusion spectrum behind a lithium-bearing blanket. Figure 4 shows the radial attenuation of the total flux across the inboard build between the two tallied zone points: the flux falls by a factor $\sim$**4.3** from the first wall to the breeder zone, the softening that both moderates the neutrons for ^{6}Li capture and protects the inboard structure.

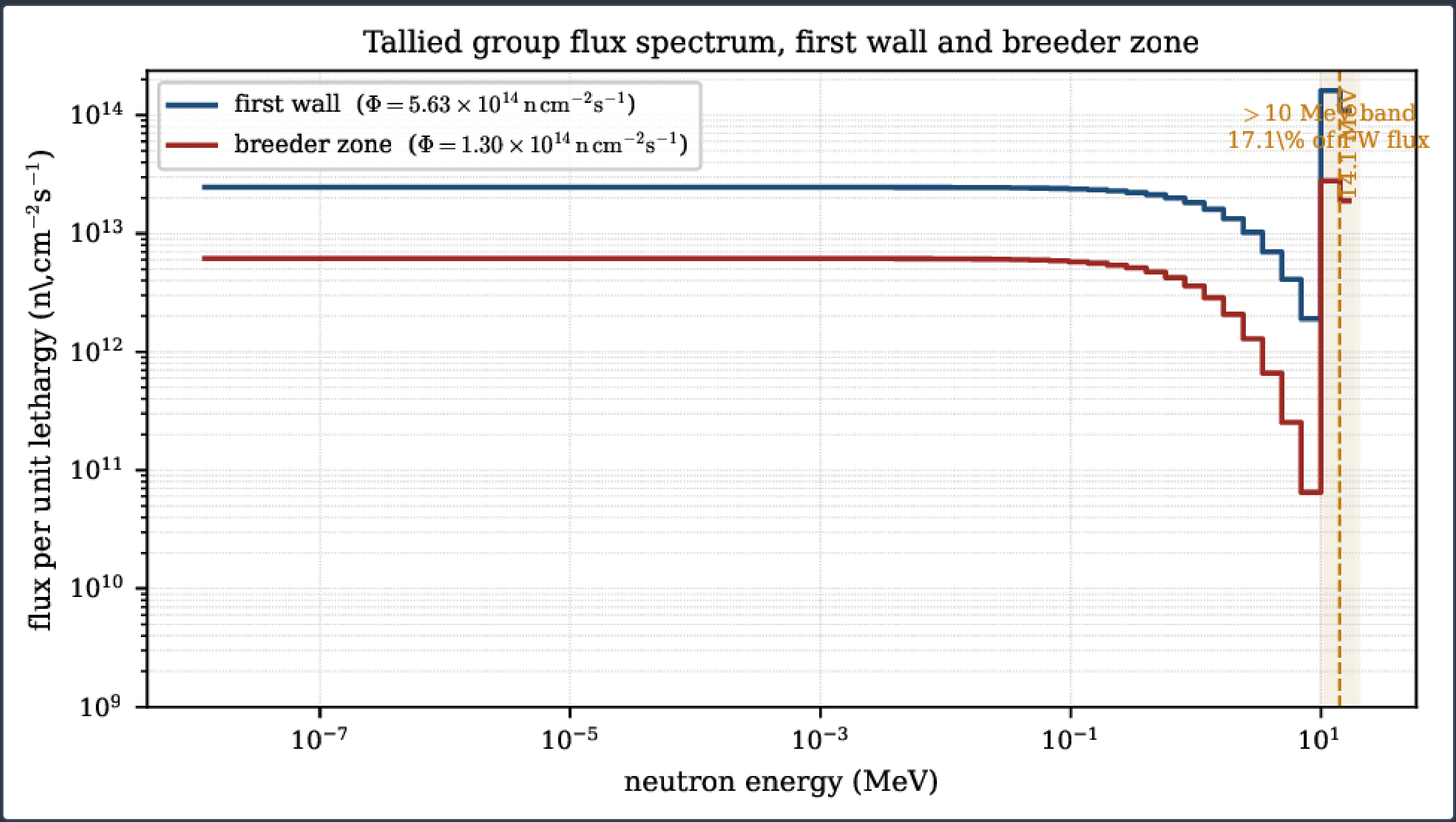

Tallied **175**-group neutron flux spectrum at the first wall (blue) and in the breeder zone (red), per unit lethargy. The total flux and the **17.1%** fraction above **10** MeV are the tallied integral values (serial BR-L2-A23); the **14.1** MeV peak and slowing-down tail are the representative VITAMIN-J spectral shape. *(Schematic group shape; integral flux and 14 MeV-band fraction are tallied.)*

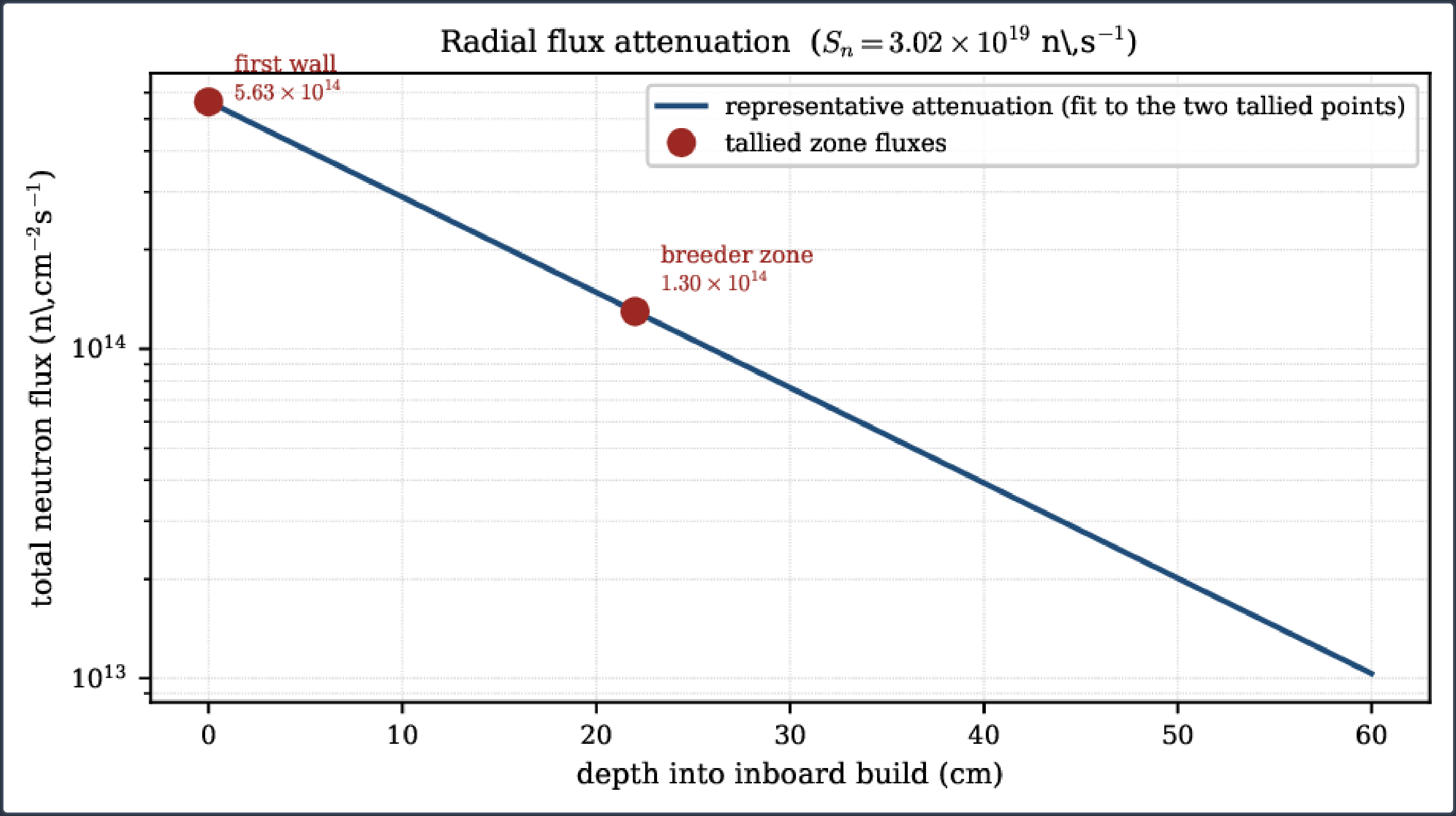

Radial attenuation of the total neutron flux across the inboard build, anchored on the two tallied zone fluxes (first wall 5.63×10^{14} $cm^{-2}s^{-1}$; breeder zone 1.30×10^{14} $cm^{-2}s^{-1}$; serial BR-L2-A23) with a representative single-exponential attenuation fit to the two points. Source strength $S_n = 3.02 \times 10^{19}$ n s^{-1}.

THE ACTIVATION INVENTORY

Table 2 reports the transport-driven activation of the first wall (Eurofer) and the breeder zone after one full-power year, at shutdown, one year and one century. Figure 5 shows the decay-heat trajectory and Figure 6 the specific activity, both falling by many orders of magnitude from shutdown to a century. First-wall decay heat falls from 56.0 W kg^{-1} at shutdown to 1.22 W kg^{-1} at one year and 2.4×10^{-8} W kg^{-1} at a century; the breeder zone falls from 29.2 to 0.20 W kg^{-1} and 2.1×10^{-4} W kg^{-1} on the same schedule. Figure 7 resolves the first-wall decay heat into a representative nuclide decomposition consistent with the identified dominant contributors: short-lived ^{56}Mn ($T_{1/2} = 2.58$ h) and ^{52}V (3.7 min) at shutdown; ^{51}Cr (27.7 d), ^{54}Mn (312 d) and ^{55}Fe (2.74 y) through the first year; and a residual ^{3}H/^{53}Mn tail by a century.

ZONE / COOLING TIME	SPECIFIC ACTIVITY (BQ KG^{-1})	DECAY HEAT (W KG^{-1})	CLASS-C WDR INDEX
first wall, shutdown	2.64×10^{14}	56.0	1.5×10^{-5}
first wall, 1 y	7.13×10^{13}	1.22	1.5×10^{-5}
first wall, 100 y	2.70×10^{7}	2.4×10^{-8}	1.5×10^{-5}
breeder zone, shutdown	2.34×10^{14}	29.2	2.6×10^{-3}
breeder zone, 1 y	6.55×10^{13}	0.20	2.6×10^{-3}
breeder zone, 100 y	2.33×10^{11}	2.1×10^{-4}	2.6×10^{-3}

Post-shutdown activation of the first wall (Eurofer) and breeder zone after one full-power year, from the transport-driven ALARA solution normalised to $P_{fus} = 85.04$ MW (serial BR-L2-A23). The Class-C waste-disposal rating (Eq. 10) stays far below the boundary ($WDR_C = 1$) in both zones at all cooling times.

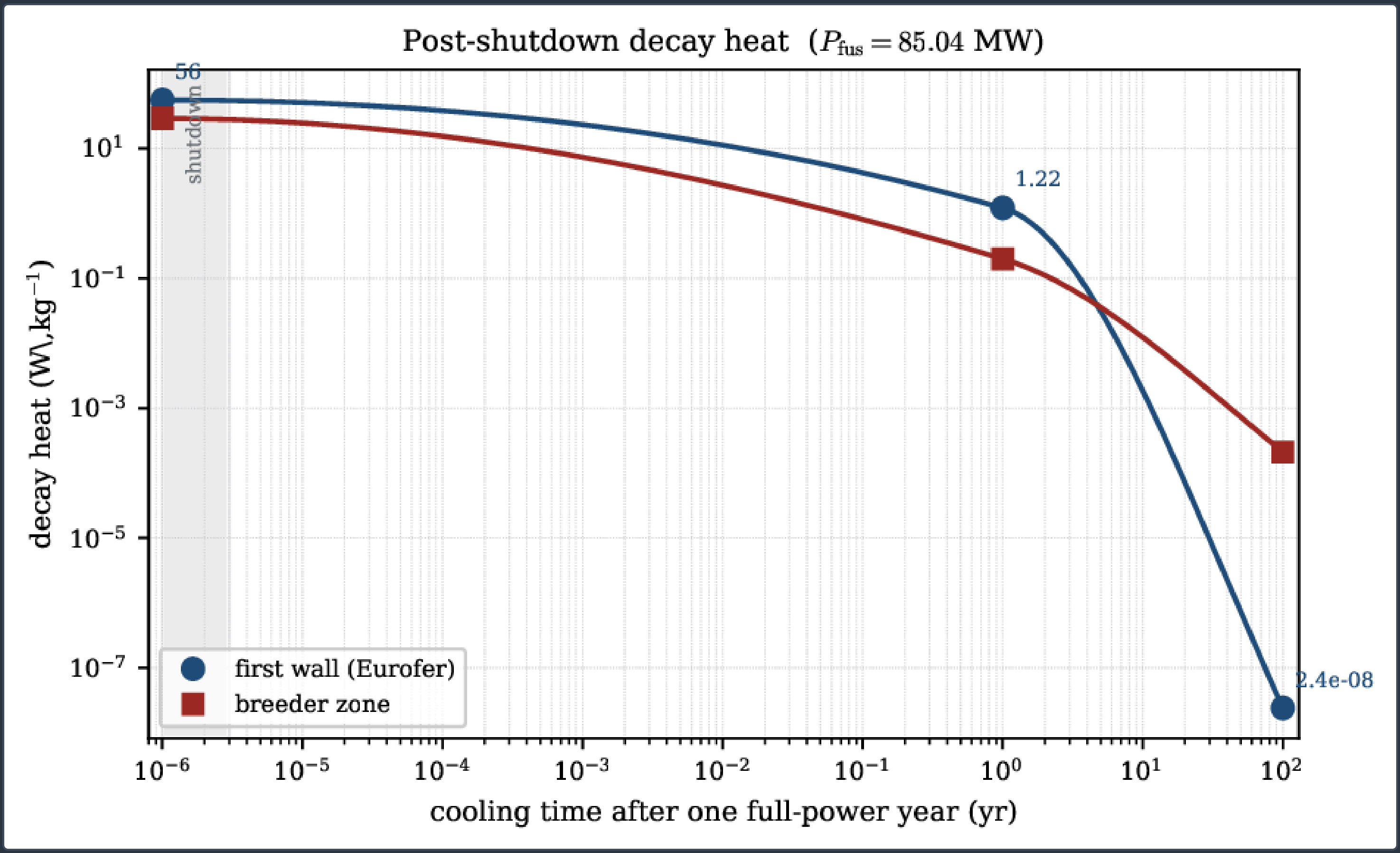

Post-shutdown decay heat of the first wall and breeder zone versus cooling time after one full-power year, normalised to $P_{fus} = 85.04$ MW. Markers are the tabulated ALARA values (Table 2); curves are a monotone log–log interpolation through them. Data: serial BR-L2-A23.

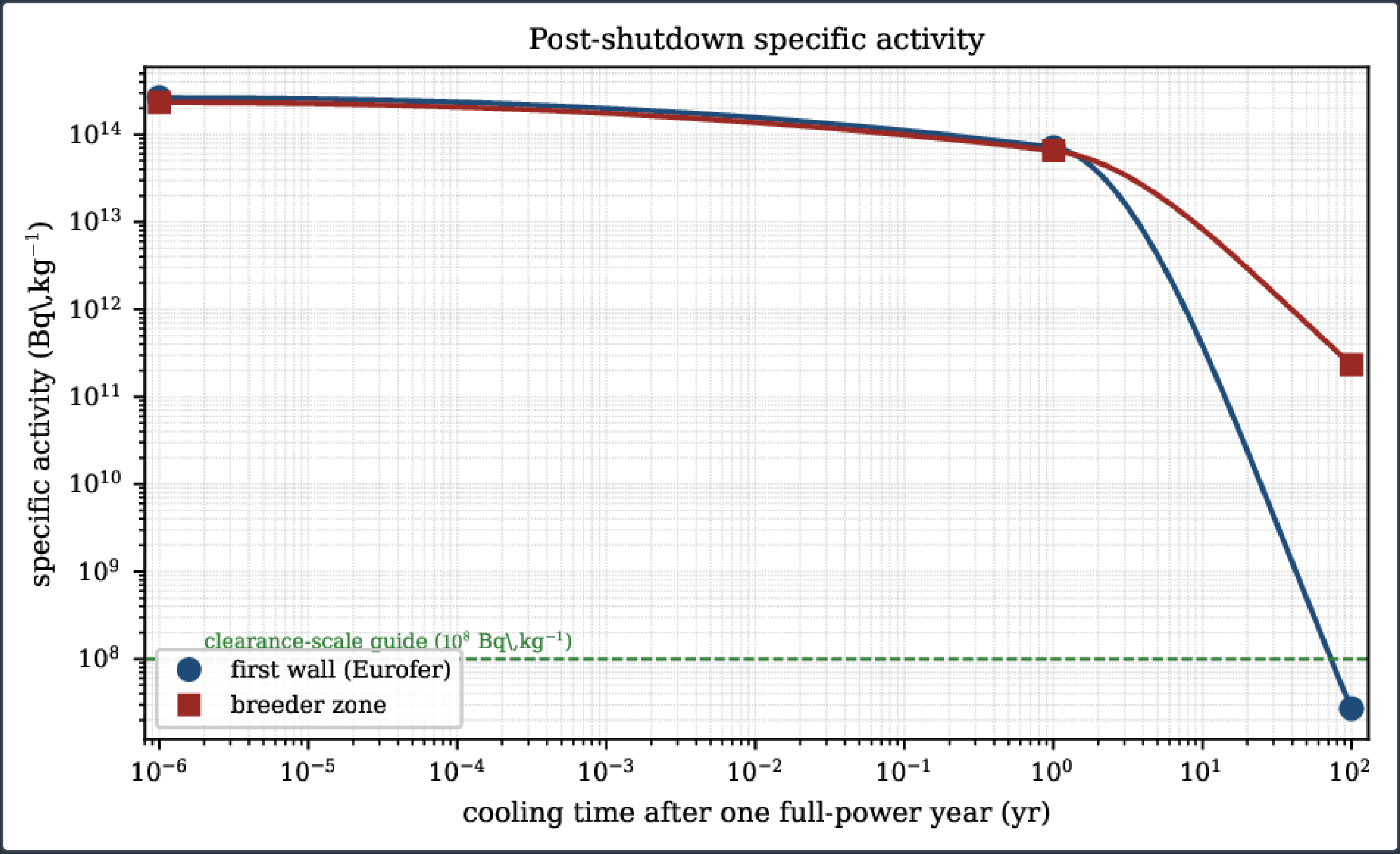

Post-shutdown specific activity of the first wall and breeder zone versus cooling time; markers are the tabulated ALARA values, curves the log–log interpolation. The first wall falls below the 10^8 Bq kg^{-1} clearance-scale guide within decades. Data: serial BR-L2-A23.

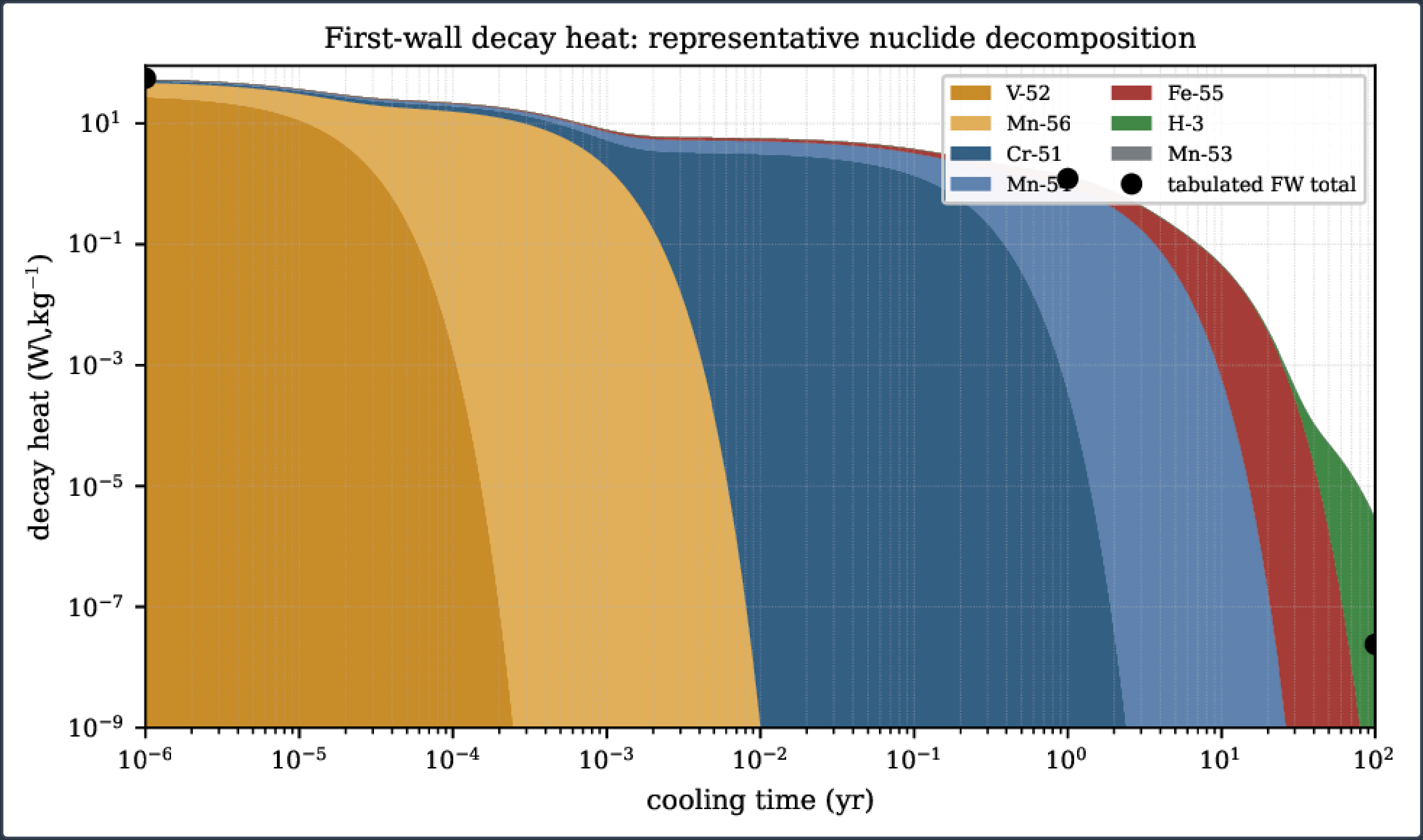

First-wall decay heat resolved into a representative nuclide-by-nuclide decomposition using the identified dominant contributors and their tabulated half-lives, normalised so the stacked total tracks the tabulated first-wall anchors (black markers). ^{56}Mn/^{52}V dominate at shutdown, ^{51}Cr/^{54}Mn/^{55}Fe through the first year, and a ^{3}H/^{53}Mn residue remains at a century. *(Representative decomposition consistent with the identified nuclides; totals are the tallied values.)*

THE WASTE-CLASS VERDICT

The strongest single outcome is the waste class. Figure 8 plots the Class-C WDR index of Eq. 10 for both zones at all three cooling times against the Class-C boundary. The index stays at or below 2.6×10^{-3} in *every* zone at *every* cooling time — more than two orders of magnitude inside the boundary, with no long-lived class driver in the modelled composition. The structure is low-level waste at discharge and decays toward clearance-scale inventories within decades; consistent with the component activation and waste-routing companion [28], tritium management rather than structural activation sets the handling class.

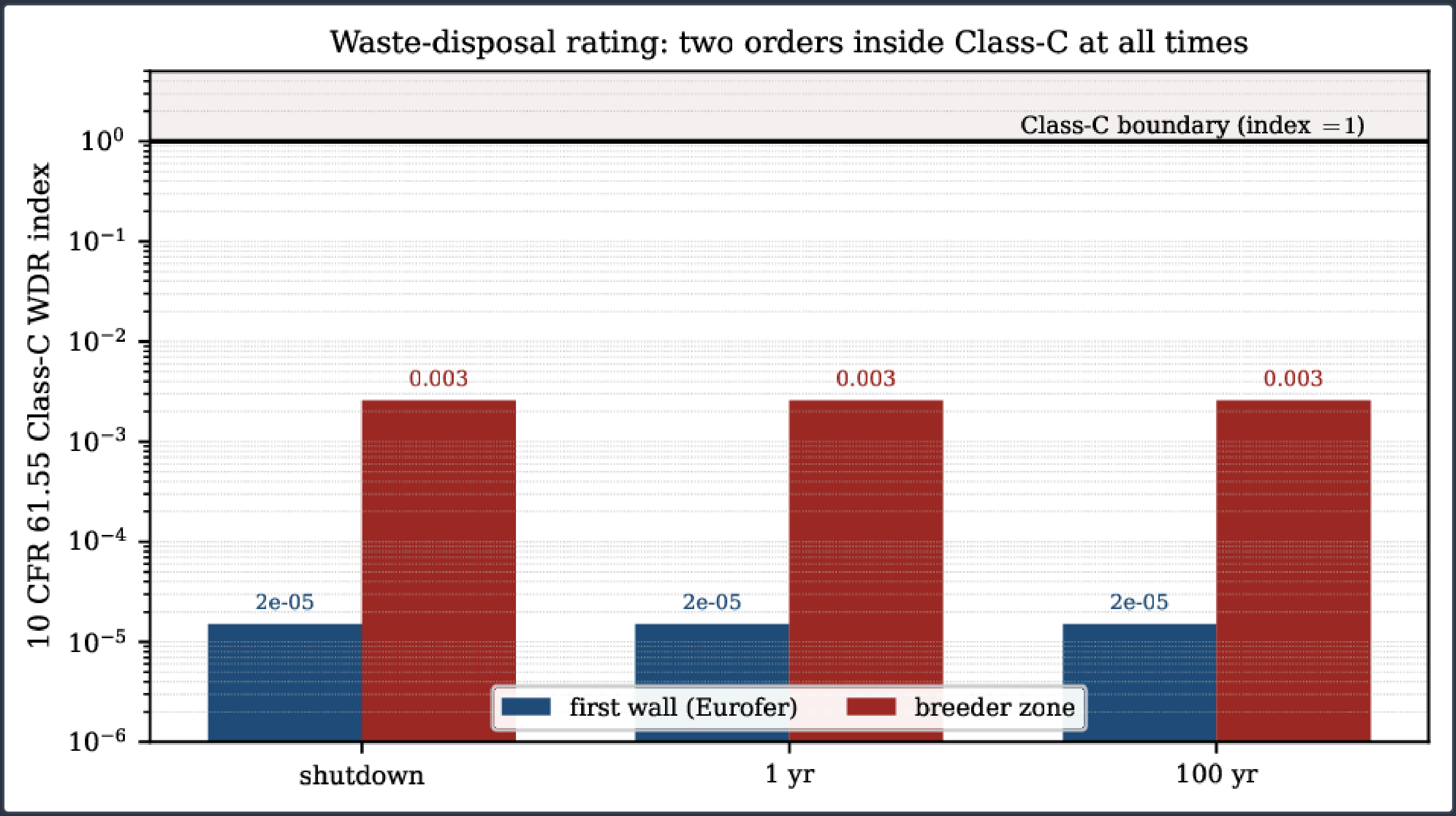

Class-C waste-disposal-rating index (Eq. 10) for the first wall and breeder zone at shutdown, 1 yr and 100 yr, against the Class-C boundary (index $= 1$, black line). Both zones stay at or below 2.6×10^{-3} at all times: low-level waste, nothing greater-than-Class-C. Data: serial BR-L2-A23.

THE TWIN AND ITS MATURITY GATE

Figure 9 illustrates the acceptance test of Eq. 13: a fast surrogate tracks a tracked neutronic index against a reference OpenMC calculation, holds authority while it stays within the $\pm 5\%$ band, and abstains to a conservative deterministic floor when an excursion carries it out of band. This is the mechanism by which the twin's live tritium-production, damage and waste indices are made trustworthy rather than merely fast, and it binds the twin to the same verification pedigree as the codes that produced Tables 1–2.

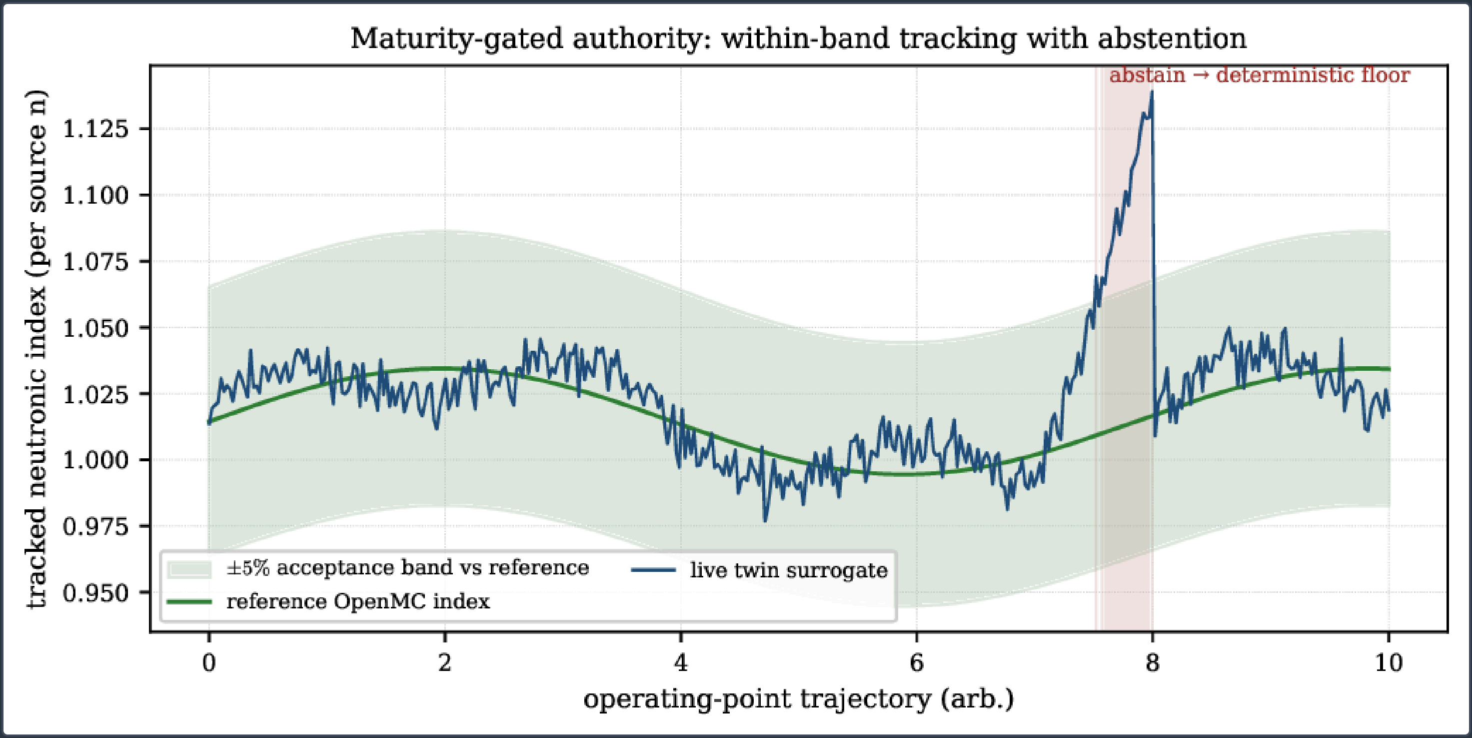

Maturity-gated authority. The live twin surrogate (blue) tracks a reference OpenMC neutronic index (green) as the operating point moves; authority is held while the surrogate stays inside the $\pm 5\%$ acceptance band (Eq. 13) and is handed to a deterministic floor during the out-of-band excursion (red). *(Schematic illustration of the acceptance criterion.)*

§ 6

Discussion

THE WASTE RESULT AGAINST THE PUBLISHED BENCHMARKS

The headline waste verdict is quantitatively strong against the fusion-waste literature. The 10 CFR 61.55 sum-of-fractions of Eq. 10 is the same functional used since Fetter, Cheng and Mann's long-term fusion-waste analyses [4], and the reduced-activation ferritic–martensitic (RAFM) structural choice is precisely the material class developed to keep that functional small [21,20]. A Class-C index of $\leq 2.6 \times 10^{-3}$ — two-to-three orders of magnitude inside the boundary — places the Kronos breeder structure firmly in the low-level, non-GTCC regime that the RAFM programme targets, and is consistent with the component-level waste-routing analysis of the companion paper [28]. The result matters for the compact-ST licensing thesis: a sub-100 MW breeder whose activation stays two orders inside Class-C strengthens the byproduct-material posture rather than the reactor-licensing one.

THE DECAY-HEAT TRAJECTORY AND THE SAFETY CASE

The decay-heat trajectory — $56.0 \to 1.22$ W kg^{-1} over the first year at the first wall — is favourable for the walk-away safety argument. The magnitude and the nuclide sequence (^{56}Mn/^{52}V $\to$ ^{51}Cr/^{54}Mn/^{55}Fe $\to$ ^{3}H/^{53}Mn) are the expected signature of a RAFM/Eurofer first wall under a 14 MeV fusion spectrum [2,23], and the century-scale reduction to 10^{-8} W kg^{-1} is what underwrites passive post-shutdown cooling. The transport-driven route used here — a three-dimensional spectrum rather than a scaled one-group flux — is what makes these numbers defensible: the same discipline that the ITER E-lite model brings to whole-device dose mapping [18], applied to a compact ST activation inventory.

DISPLACEMENT DAMAGE AND THE COUPLED STATE

The activation inventory is one projection of the neutron field; the displacement-damage field is another, and the twin tracks both from the same spectrum. The dpa rate follows from the same group flux through the NRT kernel [19] with the arc-dpa correction [3], and the fast-fluence budget it accumulates is what sets the consumable-centrepost replacement cadence analysed in the companion life-limiter study [31]. Because breeding (Eq. 5), heating (Eq. 5), activation (Eq. 6) and damage all derive from the one flux, the twin's value is precisely that it keeps them mutually consistent as the operating point moves — which a set of independent static reports cannot guarantee.

R2S IN CONTEXT

Closing the R2S loop places the twin in the same methodological family as the reference shutdown-dose systems R2S [5] and R2SUNED [6], with the deep-penetration dose problem made tractable by global variance reduction [17]. The distinguishing feature here is not the method but the coupling: the activation inventory that defines the photon source of Eq. 11 is computed per zone and per cooling time as an intrinsic output of the twin, so the photon-transport step is a direct continuation of the same verified pipeline rather than a separate study. Occupational dose around penetrations and ducts — the streaming paths that dominate the maintenance dose — is treated in the companion streaming analysis [29] on the same geometry.

§ 7

Limitations

One honest gate remains. The demonstrated activation inventory uses a truncated ($Z \leq 30$) sample cross-section library, so the first-decade first-wall inventory is a conservative lower bound until the full FENDL-3.2/EAF-2010 library folds in the tungsten and tantalum transmutation channels of the plasma-facing surface. The waste *classification* is far less sensitive to this truncation than the absolute inventory: the Class-C margin of Eq. 10 is so large ($\leq 2.6 \times 10^{-3}$) that the low-level, non-GTCC conclusion is robust to the missing high-Z channels, which contribute short-to-intermediate-lived activity rather than a long-lived Class-C driver. The full library is a defined next input to the same frozen pipeline, not an open physics question; its effect is to raise the early first-wall decay heat toward its true value while leaving the waste-class verdict and the R2S dose schedule intact.

§ 8

The neutronics and activation twin

The two demonstrated legs support a single object. The neutronics/activation twin runs the CAD-faithful transport of Eq. 2 and the ALARA activation of Eq. 6 against the live operating state, so that tritium production, displacement damage, activation inventory and — with the photon step of Eq. 12 — shutdown dose all track the operating point rather than a nominal snapshot. Its admission to control authority is the pre-registered inequality of Eq. 13: the live indices must stay within 5% of a reference OpenMC calculation, with abstention to a deterministic floor otherwise — the same maturity gate the four-twin architecture applies to its other domains [32]. The twin is the shadow that keeps the machine's neutronic state a known, verified quantity as the operating point moves.

§ 9

Conclusion

A neutronics-and-activation digital twin needs a geometry it can trust and a source it computes from, and both are demonstrated here. The CAD-faithful STEP $\to$ DAGMC $\to$ OpenMC chain reproduces the reference geometry exactly ($r_V = 1.000000$, seven digits) with physically-sensible verification-shell tallies (tritium production 1.0145 ± 0.0039 per source neutron, heating $12.63\,\mathrm{MeV\,n^{-1}}$, leakage 0.1505 ± 0.0013), and the transport-driven ALARA inventory — normalised to $P_{\mathrm{fus}} = 85.04\,\mathrm{MW}$ and $S_{\mathrm{n}} = 3.02 \times 10^{19}\,\mathrm{n\,s^{-1}}$ — gives first-wall decay heat falling to $1.22\,\mathrm{W\,kg^{-1}}$ at one year and a Class-C waste-disposal-rating index held at or below 2.6×10^{-3} in every zone at every cooling time: low-level waste at discharge, nothing greater-than-Class-C. On these two legs, joined by the rigorous-two-step loop, the twin tracks the breeder's coupled neutronic state — breeding, damage, activation and shutdown dose — as one verified pipeline, and the photon-transport step completes the shutdown-dose map on the staged schedule.

Acknowledgments tocsectionAcknowledgments Part of the Kronos Fusion Energy 2026 design series. The neutron-transport, activation and shutdown-dose calculations were performed on the NVIDIA GPU HPC campaign.

Reproducibility tocsectionReproducibility This paper is archived at doi:10.5281/zenodo.22645878; official version: https://www.kronosfusionenergy.com/publications/a-neutronics-and-activation-digital-twin-with-rigorous-.html and its official version is hosted at https://www.kronosfusionenergy.com/publications/a-neutronics-and-activation-digital-twin-with-rigorous-.html. The CAD-faithful transport chain (serial BR-L2-A22; STEP $\to$ DAGMC $\to$ OpenMC) and the activation/R2S inventory (serial BR-L2-A23; ALARA on 175-group VITAMIN-J spectra) are frozen results in the Kronos Physics De-Risking Register (doi:10.5281/zenodo.22133057), regenerable byte-for-byte from the archived drivers, input decks, data-library versions and random-number seeds, and gated by an independent-library reproduction. The figure-generation script is archived with the deposit.

Data availability tocsectionData availability This paper is archived at doi:10.5281/zenodo.22645878. The transport and activation inputs and results are archived with the deposit and reference the Kronos 2026 series register doi:10.5281/zenodo.22133057. Any economic analysis is reported separately and is not included in the public deposit.

Competing interests tocsectionCompeting interests Provisional patent applications relating to aspects of this work have been filed.

APPARATUS

Portfolio, People & Record

The intellectual-property estate, the people who built it, the limitations that gate it, and the sources it rests on.

1	4	40	27
GRANTED PATENT	2026 PROVISIONALS	TEAM MEMBERS	2022 PROVISIONALS

INTELLECTUAL PROPERTY

The patent portfolio

The estate spans a granted high-field magnet patent, pending utility and 2026 provisional filings that map to the two products, a digital-twin control provisional, a registered trademark application, and the original 2022 provisional family. Every patentable disclosure in the five-paper arXiv drop was protected **before** publication: the breeder and burner provisionals were filed 1–2 August, and a publication-gap omnibus filing the evening before the drop swept up the DEC, plasma-control, and REBCO-winding matter of the three otherwise-unprotected papers. Patent numbers and application serials are matters of public record; claim scope is summarised, not reproduced.

GRANTED & PENDING UTILITY

US 12,009,112	High-field tilted graded-REBCO magnet architecture (KRONO-002A) · *app. 17/878,550*	GRANTED
US 17/878,507	Core device / method (KRONO-001A) · *utility*	PENDING

2026 PROVISIONAL FILINGS — MAPPED TO THE PRODUCTS

64/124,209	Hyperion — spherical-tokamak tritium / helium-3 foundry · *breeder · filed Aug 2026*	FILED
64/124,220	Aegis / MetroVolt — synchrotron-cutoff, fuel-selection & plug-winding · *generator · filed Aug 2026*	FILED
64/115,167	KRONOS-CTRL digital-twin plant control · *provisional · filed Jul 2026*	FILED
64/005,440	Integrated spherical-tokamak fusion architecture · *early integrated-architecture filing · filed Mar 2026*	FILED
64/105,530	Negative-triangularity spherical-tokamak architecture · *foundational ST filing · filed Jul 2026*	FILED
64/128,097	Publication-gap omnibus — quasineutral two-species expander DEC · provenance-gated / latency-split plasma control · as-built high-field winding & conductor architecture · *filed 7 Aug 2026, the evening before the arXiv drop*	FILED

TRADEMARK & ORIGIN

FTK-98801894	Kronos Fusion Energy — trademark application	FILED
KR-2022-*	Original provisional family (KR-2022-00001 … 00027) · *27 filings, 2022*	PRIORITY

The narrow, defensible magnet novelty — the specific conductor and the digital-twin winding optimisation, not high-field REBCO as a category — is the commercial core that can earn ahead of any Q > 1 milestone, with markets in fusion magnet supply, MRI/NMR, accelerators, and proton therapy. The claim is scoped honestly: the high field is a *system field* result, not a stand-alone-coil record; the small-bore plug coil is structurally infeasible as a bare winding but resolved by a stress-managed structural shield (feasible-pending-FEA); and the winding-tape experiment returned a *null result*. The value is the method, not a field record.

THE TEAM

Founding partners, board, advisors & auditors

Kronos is built by a bench of advanced-fuel-fusion, high-field-magnet, direct-conversion, and materials specialists, with a board and operations team drawn from defense, national laboratories, and industry. Dates are shown as ranges; where a tenure has ended or is term-ending, the range says so.

FOUNDING PARTNERS — SCIENCE

Dr. Gerald Kulcinski
Co-Founder · Helium-3 & Advanced-Fuel Fusion
UW–Madison · 2023–Present

Dr. Carl Weggel
Chief Scientist / S.M.A.R.T. Design
MIT Alcator Program · 2022–Present

Dr. Robert J. Weggel
Magnetic Field Design
MIT Magnet Lab · 2022–Present

BOARD

Priyanca Ford
Founder & CEO · Executive Board
2022–Present

Bandel Carano
Finance / Strategy
Oak Investment Partners / Stanford · 2025–2026

Patrick Schweiger
Fusion Device Engineering
Oklo / CFS / TerraPower · 2025–Present

SCIENTIFIC ADVISORS

Dr. Steven O. Dean
Fusion Policy & History
DOE / Fusion Power Associates · 2025–Present

Dr. Patrick H. Diamond
Plasma Turbulence & Transport
UC San Diego · 2025–Present

Dr. Jack J. Dongarra
HPC & Numerical Algorithms
Turing Award · 2025–Present

Dr. Nasr M. Ghoniem
Chief Material Scientist
UCLA · 2025–Present

Dr. Siegfried Glenzer
Plasma Physics & Laser Fusion
Stanford / SLAC · 2022–Present

Dr. David A. Hammer
Pulsed-Power Fusion
Cornell · 2025–Present

Dr. Donald A. Spong
Plasma Theory & Confinement
ORNL · 2025–Present

Dr. Curtis Smith
Risk Assessment & Nuclear PRA
MIT / Idaho National Lab · 2025–Present

RADM (Ret.) David Goggins
Naval Engineering & Power-Plant Design
U.S. Navy · 2023–2026

Dr. Konstantin Batygin
Mathematician
Caltech · 2022–2025

Dr. Ruben Fair
Magnet Design / ITER Liaison
PPPL / Jefferson Lab · 2022–2025

Dr. Paul S. Weiss
Materials & Nanotechnology
UCLA · 2022–2025

SCIENTIFIC AUDITORS

Dr. Wilfred A. Cooper
Plasma Equilibrium Theory
EPFL / Swiss Plasma Center · 2025–Present

Dr. Ahmed Hassanein
Plasma–Material Interactions
Purdue / Argonne · 2025–Present

Dr. Patrick E. Hopkins
Extreme Thermal Materials
U. of Virginia · 2025–Present

Dr. Peter Hosemann
Materials Joining & Structural Integrity
UC Berkeley · 2025–Present

Dr. Travis W. Knight
Advanced Nuclear Fuels & Systems
U. of South Carolina · 2025–Present

Dr. Philippe Lebrun
Cryogenics & Magnet Cooling
CERN · 2025–Present

Dr. Nitendra Singh
Nuclear Safety & Fuel Cycle
ITER · 2025–Present

Dr. Guido Van Oost
Magnetic Confinement & Fusion Systems
Ghent University · 2025–Present

Dr. Gary S. Was
Radiation Materials & Structural Integrity
U. of Michigan · 2025–Present

Dr. Ray Sedwick
Direct Energy Conversion
U. of Maryland · 2025

OPERATIONS

Michael Laughlin
Chief Operating Officer
2022–Present

Martin Owens
Chief Strategy Officer
LANL / GE Hitachi · 2022–Present

MG (Ret.) Paul Pardew
Chief Contracting Officer
Army Contracting Command · 2022–Present

David Beck
Fusion Commercialization
U.S. Space Force · 2024–Present

Sushma Bhatia
Environmental & Legislative
Google · 2022–Present

Michael De Frenza
Technology Licensing
2023–Present

MG (Ret.) Robin L. Fontes
Cybersecurity & Defense
Army Cyber Command · 2022–Present

Vijay Gehani
Supply Chain & Components
INOX India · 2024–Present

Jon Michel Greenwood
IT & AI Infrastructure
Live Nation · 2023–Present

Brian C. O'Neill
National Security
CIA / ODNI · 2022–Present

Gen. (Ret.) Gustave F. Perna
DoD Liaison
Operation Warp Speed · 2022–2023

Andrea Romero
Marketing Lead
2022–Present

Legal counsel is retained; those roles are held on the internal roster and are not listed here.

SOURCES

References

1 H-S Bosch and G M Hale, Improved formulas for fusion cross-sections and thermal reactivities, *Nucl. Fusion* **32** 611 (1992). doi:10.1088/0029-5515/32/4/I07

2 M R Gilbert, S L Dudarev, S Zheng, L W Packer and J-Ch Sublet, An integrated model for materials in a fusion power plant: transmutation, gas production, and helium embrittlement under neutron irradiation, *Nucl. Fusion* **52** 083019 (2012). doi:10.1088/0029-5515/52/8/083019

3 K Nordlund *et al*, Improving atomic displacement and replacement calculations with physically realistic damage models, *Nat. Commun.* **9** 1084 (2018). doi:10.1038/s41467-018-03415-5

4 S Fetter, E T Cheng and F M Mann, Long-term radioactive waste from fusion reactors: Part II, *Fusion Eng. Des.* **13** 239 (1990). doi:10.1016/0920-3796(90)90104-E

5 Y Chen and U Fischer, Rigorous MCNP based shutdown dose rate calculations: computational scheme, verification calculations and application to ITER, *Fusion Eng. Des.* **63–64** 107 (2002). doi:10.1016/S0920-3796(02)00144-8

6 P Sauvan, J P Catalan, F Ogando, R Ju\'arez and J Sanz, Development of the R2SUNED code system for shutdown dose rate calculations, *IEEE Trans. Nucl. Sci.* **63** 375 (2016). doi:10.1109/TNS.2015.2507138

7 J E Menard *et al*, Fusion nuclear science facilities and pilot plants based on the spherical tokamak, *Nucl. Fusion* **56** 106023 (2016). doi:10.1088/0029-5515/56/10/106023

8 B N Sorbom *et al*, ARC: a compact, high-field, fusion nuclear science facility and demonstration power plant with demountable magnets, *Fusion Eng. Des.* **100** 378 (2015). doi:10.1016/j.fusengdes.2015.07.008

9 M G Kapteyn, J V R Pretorius and K E Willcox, A probabilistic graphical model foundation for enabling predictive digital twins at scale, *Nat. Comput. Sci.* **1** 337 (2021). doi:10.1038/s43588-021-00069-0

10 P K Romano, N E Horelik, B R Herman, A G Nelson, B Forget and K Smith, OpenMC: a state-of-the-art Monte Carlo code for research and development, *Ann. Nucl. Energy* **82** 90 (2015). doi:10.1016/j.anucene.2014.07.048

11 P K Romano, C J Josey, A E Johnson and J Liang, Depletion capabilities in the OpenMC Monte Carlo particle transport code, *Ann. Nucl. Energy* **152** 107989 (2021). doi:10.1016/j.anucene.2020.107989

12 J Lepp\"anen, M Pusa, T Viitanen, V Valtavirta and T Kaltiaisenaho, The Serpent Monte Carlo code: status, development and applications in 2013, *Ann. Nucl. Energy* **82** 142 (2015). doi:10.1016/j.anucene.2014.08.024

13 P P H Wilson, T J Tautges, J A Kraftcheck, B M Smith and D L Henderson, Acceleration techniques for the direct use of CAD-based geometry in fusion neutronics analysis, *Fusion Eng. Des.* **85** 1759 (2010). doi:10.1016/j.fusengdes.2010.05.030

14 J-Ch Sublet, J W Eastwood, J G Morgan, M R Gilbert, M Fleming and W Arter, FISPACT-II: an advanced simulation system for activation, transmutation and material modelling, *Nucl. Data Sheets* **139** 77 (2017). doi:10.1016/j.nds.2017.01.002

15 D A Brown *et al*, ENDF/B-VIII.0: the 8th major release of the nuclear reaction data library with CIELO-project cross sections, new standards and thermal scattering data, *Nucl. Data Sheets* **148** 1 (2018). doi:10.1016/j.nds.2018.02.001

16 M Angelone *et al*, Benchmarking of the FENDL-3 neutron cross-section data starter library for fusion applications, *Nucl. Data Sheets* **120** 245 (2014). doi:10.1016/j.nds.2014.07.054

17 A Davis and A Turner, Comparison of global variance reduction techniques for Monte Carlo radiation transport simulations of ITER, *Fusion Eng. Des.* **86** 2698 (2011). doi:10.1016/j.fusengdes.2011.01.059

18 R Ju\'arez *et al*, A full and heterogeneous model of the ITER tokamak for comprehensive nuclear analyses, *Nat. Energy* **6** 150 (2021). doi:10.1038/s41560-020-00753-x

19 M J Norgett, M T Robinson and I M Torrens, A proposed method of calculating displacement dose rates, *Nucl. Eng. Des.* **33** 50 (1975). doi:10.1016/0029-5493(75)90035-7

20 G Federici, L Boccaccini, F Cismondi, M Gasparotto, Y Poitevin and I Ricapito, An overview of the EU breeding blanket design strategy as an integral part of the DEMO design effort, *Fusion Eng. Des.* **141** 30 (2019). doi:10.1016/j.fusengdes.2019.02.013

21 E Gaganidze and J Aktaa, Assessment of neutron irradiation effects on RAFM steels, *Fusion Eng. Des.* **88** 118 (2013).

22 M E Sawan and M A Abdou, Physics and technology conditions for attaining tritium self-sufficiency for the DT fuel cycle, *Fusion Eng. Des.* **81** 1131 (2006).

23 M R Gilbert, J-Ch Sublet and S L Dudarev, Neutron-induced dpa, transmutation, gas production, and helium embrittlement of fusion materials, *J. Nucl. Mater.* **442** S755 (2013).

24 U.S. Nuclear Regulatory Commission, Title 10, Code of Federal Regulations, §61.55, Waste classification (Licensing requirements for land disposal of radioactive waste).

25 ASTM International, ASTM E521, Standard Practice for Investigating the Effects of Neutron Radiation Damage Using Charged-Particle Irradiation, ASTM, West Conshohocken PA.

26 P I Ford, Hyperion as a strategic-materials platform: gain, tritium breeding, He-3 co-production, and 14 MeV neutron output from a compact spherical tokamak, Kronos Fusion Energy 2026 series. doi:10.5281/zenodo.22645691. https://www.kronosfusionenergy.com/publications/breeder.html

27 P I Ford, CAD-faithful neutronics for a compact spherical-tokamak breeder: STEP-to-DAGMC Monte-Carlo transport reproducing the 3-D net tritium-breeding ratio, Kronos Fusion Energy 2026 series. doi:10.5281/zenodo.22645881. https://www.kronosfusionenergy.com/publications/cad-faithful-neutronics-for-a-compact-spherical-tokamak.html

28 P I Ford and G L Kulcinski, Component activation, waste-class routing, and decommissioning of a low-activation compact spherical-tokamak breeder: no isotope beyond a century's half-life, Kronos Fusion Energy 2026 series. doi:10.5281/zenodo.22645846. https://www.kronosfusionenergy.com/publications/component-activation-waste-class-routing-and-decommissi.html

29 P I Ford, Neutron streaming, duct and port penetrations, and occupational dose around a 14 MeV compact spherical-tokamak breeder, Kronos Fusion Energy 2026 series. doi:10.5281/zenodo.22645842. https://www.kronosfusionenergy.com/publications/neutron-streaming-duct-and-port-penetrations-and-occupa.html

30 P I Ford, Nuclear-data uncertainty quantification for tritium breeding: which 14 MeV cross-section channels set the error bar on the breeding ratio, Kronos Fusion Energy 2026 series. doi:10.5281/zenodo.22645777. https://www.kronosfusionenergy.com/publications/nuclear-data-uq-for-the-tbr.html

31 P I Ford, The centrepost life-limiter: fast-fluence, dpa, and shielding setting the cartridge-replacement cadence for a compact spherical-tokamak breeder, Kronos Fusion Energy 2026 series. doi:10.5281/zenodo.22645708. https://www.kronosfusionenergy.com/publications/centrepost-fluence-and-shielding.html

32 P I Ford, Four coupled digital twins for a compact spherical-tokamak breeder: multi-rate co-simulation, propagated uncertainty, and a real-time self-consistency monitor, Kronos Fusion Energy 2026 series. doi:10.5281/zenodo.22645805. https://www.kronosfusionenergy.com/publications/four-coupled-digital-twins-for-a-compact-spherical-toka.html

33 P I Ford, Verification-first fusion modeling: frozen anchors, independent-library gate reproduction, and a byte-for-byte computational-provenance catalog for a breeder-and-burner design register, Kronos Fusion Energy 2026 series. doi:10.5281/zenodo.22645710. https://www.kronosfusionenergy.com/publications/verification-and-validation-47-code-provenance.html

34 P I Ford, *Kronos Physics De-Risking Register*, Kronos Fusion Energy 2026 series. doi:10.5281/zenodo.22133057.

COLOPHON

How this document was made

The Kronos Fleet — Combined Editorial, 2026 is set in **Fraunces** (display), **Gelasio** (text), and **IBM Plex Mono** (data & equations), carried forward from the Kronos editorial design system.

The figures are rendered at 300 dpi from the deposited generator scripts; the document is composed as a single self-contained file with embedded fonts and imagery, paginated to US Letter, and rendered to PDF through a headless Chromium engine in matched light and dark editions.

Every headline quantity carries an evidence class; withdrawn and restated values are marked as such. Nothing herein is frozen beyond the founder-approved Tier-A set.

Explore it live — turn the interactive 3-D model, run the deposited solvers in the physics validator, and watch the companion film series.

LEGAL NOTICE

Notice, status, and distribution

Conceptual design & simulation study. This document reports a conceptual design and simulation study. It is not a construction commitment, a safety-analysis report, a regulatory filing, or an offer of securities. Forward-looking statements — schedules, costs, market sizes, and performance — are estimates subject to the limitations set out in the Simulations part and may change.

Numbers and their classes. Quantities are reported with evidence classes and case labels; modelled, assumed, and requirement-class values are identified as such and are not to be quoted without their labels.

Public edition. This edition carries the physics and design only; all financial, funding, and defense-commercial content has been removed for public distribution. The scientific text corresponds to the arXiv and journal submissions.

THE 2026 KRONOS SERIES

One programme, many papers

This editorial is one paper in the Kronos 2026 series — a real fusion company's complete, reproducible physics record for a spherical-tokamak breeder and its low-neutron D–^{3}He tandem-mirror burners. Every headline number is a frozen anchor in the Physics De-Risking Register.

Explore the whole programme: the De-Risking Register, the interactive 3-D model, and the physics validator.

KRONOS FUSION ENERGY

A Neutronics and Activation Digital Twin with Rigorous-Two-Step Shutdown-Dose Mapping for a Compact Spherical-Tokamak Breeder

A real fusion company building real machines. Explore the science, live.

Zenodo · doi:10.5281/zenodo.22645878

Read on kronosfusionenergy.com

The Physics De-Risking Register